Digital Mammographic Computer Aided Diagnosis (CAD) using Adaptive Level Set Segmentation

John E. Ball, *Graduate Student Member*, *IEEE*, Lori Mann Bruce, Senior Member, *IEEE*

Abstract—We present a mammographic computer aided diagnosis (CAD) system, which uses an adaptive level set segmentation method (ALSSM), which segments suspicious masses in the polar domain and adaptively adjusts the border threshold at each angle to provide high-quality segmentation results. The primary contribution of this paper is the adaptive speed function for controlling level set segmentation. To assess the efficacy of the system, 60 relatively difficult cases (30 benign, 30 malignant) from the Digital Database of Screening Mammography (DDSM) are analyzed. The segmentation efficacy is analyzed qualitatively via visual inspection and quantitatively via the area under the receiver operating characteristics (ROC) curve (A_Z) and classification accuracies. For the ALSSM, the best results are 87% overall accuracy, A_Z=0.9687 with 28/30 malignant cases detected. The qualitative and quantitative results show that the ALSSM provides excellent segmentation and classification results and compares favorably to previous CAD systems in the literature which also used the DDSM database.

Keywords—Adaptive systems, Breast Cancer, Cancer, Classification, Computer Aided Diagnosis, Discriminant Analysis, Digital Mammography, Feature Extraction, Image enhancement, Image segmentation, Level Sets, Mammography, Receiver Operating Characteristics, Tumor

I. INTRODUCTION

Breast cancer is the number one leading type of women's cancer, and the second most fatal type of women's cancer, according to the American Cancer Society [3]. Mammograms are currently considered to be the best method for early detection of breast cancer [7,8]. In this letter, a digital mammography computer aided diagnosis (CAD) system using level set segmentation is investigated. This work stems from previous research of the authors [11], where simple statistical methods were used for image segmentation, and from the authors previous experience using level sets for remote sensing image segmentation [15-18].

Mammograms often have poor contrast and need noise reduction and image enhancement in order for a CAD system to be able to perform a good image analysis. Pisano *et al.* concluded that contrast limited adaptive histogram equalization (CLAHE) "… might be helpful in allowing radiologists to see subtle edge information, such as spiculations" [20]. Other image preprocessing methods are fuzzy transformations, convolution with an isotropic Gaussian kernel, and wavelet and multi-scale enhancement.

There are many approaches to mammographic mass segmentation, including morphological texture features, gray level image statistics, fuzzy image processing, multi-resolution analysis, support vector machines, statistical methods, and customized filtering. Many of these approaches are summarized in [22] and discussed in detail in [23][1].

II. LEVEL SET METHODS

The 2D level set image segmentation methodology uses the zero level set of a 3D implicit function, ϕ, defined as $\phi(x,y,t):\Re^2 \times [0,T] \to \Re$, where T is some large maximum time value for the system. The segmentation boundary is controlled by the following partial differential equation (PDE), $\phi_t + \boldsymbol{F}|\nabla \phi| = 0$, where ϕ_t is the partial derivative of ϕ with respect to time, $\nabla \phi$ is the gradient of ϕ, and the time variable, t, is used in numerical evaluation of the PDE [24]. The speed function, $\boldsymbol{F}$, controls the level set evolution. If $\boldsymbol{F}$>0 ($\boldsymbol{F}$<0), then the level set boundary will expand outwards (inwards) normal to the boundary; if $\boldsymbol{F}$=0, then the boundary will not move. The implicit function ϕ is a signed distance function (SDF), which means that $\phi_{x,y}$ is the signed distance to the nearest segmentation boundary point from point (x,y), with a negative (positive) sign for points inside (outside) of the boundary [24].

III. DATA

A subset of the DDSM database obtained from the H. Lee Moffitt Cancer Research Center at the University of South Florida [25] is used in this research. The test data set consists of 60 test cases (30 benign, 30 malignant). Each test case consists of a mammographic image and a region of interest (ROI) template, as well as age and diagnosis data about each patient. The ROI template was created by expert radiologists and is considered to be the accurate location of the suspicious area in the mammogram. These diagnoses were validated with biopsies and follow–up visits. The original mammographic images were scanned with a Howtek scanner with a pixel size of 43.5^2 μm^2 and 12 bits per pixel

Manuscript received March 2, 2007.

J.E. Ball is with the Navy Surface Warfare Center, Dahlgren, VA 22485, USA (e-mail: john.e.ball@navy.mil).

L.M. Bruce is with the Electrical and Computer Engineering Department and the GeoResources Institute, Mississippi State University, Starkville, MS 39759, USA (e-mail: bruce@hpc.msstate.edu).

[1] Dissertations and Theses from Mississippi State Univeristy can be searched at http://www.library.msstate.edu. Select "Search for Materials" then choose Electronic Thesis and Dissertations.

radiometric resolution [25]. Each mammogram is cropped to [2048 × 2048] pixels in an area around the ROI.

IV. METHODOLOGY

The mammogram is preprocessed to remove noise and to enhance the mass. Then the suspicious mass is segmented, features are extracted and optimized, and then the classifier makes a benign or malignant decision. The proposed level set methods is denoted ALSSM.

CLAHE is used to remove noise and enhance the mammographic images. Next, a custom algorithm is used to provide non-linear enhancement. This algorithm is described in pseudo code in Fig. 1. The notation ".*" indicates element by element multiplication. Lines 2-4 perform a nonlinear adjustment to the image based on the image gray level statistics. Line 5 computes a mean value image using 16 by 16 blocks (size determined experimentally). Lines 6-9 provide further image enhancement. The function *normalize image* (NI) is used because it forces the image pixels to be in the range [0,1]. The enhancement image is created in line 9, and converted to polar in line 10.

Line 11 gauges the average rate of decay of the pixels radially away from the seed point. Line 12 determines a standard deviation for the isotropic Gaussian filter. The filter is modified so that pixels within one standard deviation of the seed pixel are not affected, but after one standard deviation, the decay becomes Gaussian. Previous researchers have used a fixed isotropic Gaussian filter [26,27]. However, better results were achieved in this study when using this modified isotropic filter. The size of the filter adapts to the characteristics of the mass under investigation (reference Fig. 1, lines 11-13). The enhanced images can be seen in Cartesian form in the third column on Fig. 3. The function '*HistogramEqualize*' is the Matlab function '*histeq*'.

A semi-automated seed point selection algorithm is used to determine the starting point for mass segmentation. A simple image thresholding algorithm with gray level regression is then run to detect areas in the image that are larger than a predefined minimum area and minimum gray level. These constraints are introduced because masses are typically medium to large sized objects in the cropped image, and masses typically appear as brighter areas on the digital mammograms [28]. The algorithm is shown in Fig. 2. The parameters N=40 quantization bins, A_{MIN}=5000 pixels and R=4 levels are experimentally determined. The function *imregionalmax* is a Matlab function.

The segmentation is performed in the polar domain. Using the seed point as the center of the polar image (i.e. zero radius), a circular region from the enhanced mammographic image is converted to the polar domain. The polar image, $P(r,\theta)$, has dimensions $[R_{MAX} \times N]$. R_{MAX} is set to 500 pixels (approximately 21.8 mm) to accommodate the images with larger masses, and the discrete angles used to create the polar image are $\theta \in \Theta = \{2\pi n/N\}$, with $n \in \{0,1,\cdots,N-1\}$, where N=2880 is the number of angles sampled in the polar image, providing a 1/8 degree angular

sampling rate, in order to have good resolution for large radii and thus handle large tumors). The segmentation algorithm uses the enhanced image pixel properties and varies the speed function according to an adaptive threshold, $t(\theta)$, $\theta \in \Theta$,

```
              Image Enhancement Pseudo Code

Inputs: I-mammogram image, seed point
Output: E- Cartesian enhanced image,P-Polar
        enhanced image

1    I_CL  ← CLAHE(I)
2    I_2 ← NI(I), µ ← mean of all pixels in I_2
3    I_3 ← NI(I_CL) .* (1-exp(-(I_2/µ)))
4    I_3 ← NI(I_3)
5    M_2 ← RM(I_3,[16 16])
6    I_4 ← NHEQ(I_3)
7    I_5 ← NI(I_3 + RM(M_2,[16 16]))
8    I_6 ← NHEQ(I_5) .* I_4
9    E ← NI(I_6)
10   P ← Polar(E) with center at seed point
11   µ(r) ← mean{P(r,θ)} for all r; µ_MAX ← max(µ)
12   σ ← smallest radius r with µ(r)≥0.4µ_MAX
```

$$13 \quad G(r,\theta) \leftarrow \begin{cases} 1 & r \leq \sigma \\ \exp\left(-0.5\left[(r-\sigma)/\sigma\right]^2\right) & r > \sigma \end{cases}$$

```
14   P(r,θ) ← P(r,θ) .* G(r,θ) for all r,θ
```

$$15 \quad P \leftarrow (P - mean(P))/std(P)$$

```
function N = NI(X) % Normalize image
 N ← X - min(X)
 N ← N / max(N)

function N = NHEQ(X) % Normalize and hist. eq.
 N ← HistogramEqualize(NI(X))

% Function to compute the regional mean
function N = RM(X,[b1,b2])
 M ← image where each pixel is mean value
     of a b1 by b2 block B in image X
 N ← M resized to size of X using 2D bilinear
     interpolation
```

Fig. 1. Image enhancement pseudo code.

which is adaptively adjusted as the level set segmentation proceeds. In order to quantify the border mathematically, a scalar border complexity measure (BCM) and is defined as follows. Let $r(\theta)$ and $r_P(\theta)$, be the current and previous iteration border radius, respectively, for $\theta \in \Theta$. Define BCM as

$$BCM = \operatorname*{mean}_{\theta}\left(\left\|\Delta r(\theta)\right\|\right), \qquad (1)$$

where the mean value is taken over $\theta \in \Theta$, $\Delta r(\theta) = r(\theta) - r_P(\theta)$ is the change in the border radius, and $\|\|$ is the absolute value operator. This method is similar to

```
        Seed Point Selection Algorithm Pseudo Code

Inputs: I-mammogram image;ROI-ROI image; N-
  Quantization bins; R-Regression levels; Amin-
  Minimum segmentation area.
Output: (x,y) - Seed point

1  P ← Quantize I to N bins
2  RMAX ← All zero image same size as I
3  For r = 1 : R
4    Set RMAX = max(RMAX, imregionalmax(q))
5    Set q = q - RMAX
6  End
7  Fill holes in RMAX
8  Remove areas smaller than Amin in RMAX
9  Remove areas in RMAX that don't overlap ROI
10 RMAX ← sign(RMAX)
11 ROI ← ROI shrunk by 20 pixels
12 Select seed point as brightest pixel in region
   and in ROI closest to centroid of ROI
13 Show user seed point and allow user to select
   from another region in RMAX if desired
```

Fig. 2. Seed point selection algorithm pseudo code.

the border regularization term in [29]. In order to provide some regularity to the segmentation procedure, a smoothed version of the border radius difference, $\Delta r_{SM}(\theta)$, is created by filtering $\Delta r(\theta)$ with a simple order $(N_S - 1)$ scaled boxcar smoothing filter with impulse response $h[n] = \frac{1}{N_S}$, $n \in \{0,1,\cdots,N_S - 1\}$. $N_S = 41$ was selected since it provides smoothing over approximately five degrees.

A DC threshold and an AC threshold are summed to create the overall pixel threshold. The AC threshold keeps small blobs that are not part of the mass from being segmented. The AC threshold is a function of angle, while the DC threshold is a constant across all angles. Both thresholds can vary as the segmentation iterations progress. The AC threshold is adjusted using

$$T_{AC}(\theta) = \alpha_{AC} \cdot sign(\Delta r_{SM}(\theta)) \cdot \left[1 - \exp\left(-0.5 \cdot \frac{\Delta r_{SM}(\theta)^2}{\sigma_{AC}^2} \right) \right], \quad (2)$$

where $sign(x) = 1$ if $x>0$, 0 if $x=0$, and -1 otherwise, and the parameters $\sigma_{AC} = 4.0$ and $\alpha_{AC} = 0.1$ are experimentally determined. The exponential term penalizes the areas changing rapidly more than the areas with little change. The DC threshold is adjusted using

$$T_{DC} = T_{DC\_PREV} - \left(\frac{clip(\Delta BCM, \beta)}{\alpha_{DC}} \right), \quad (3)$$

where T_{DC_PREV} is the DC threshold at the previous iteration, and the parameters $\alpha_{DC} = 0.1$ and $\beta = 0.1$ are

experimentally determined. The function $clip(a,b)$ clips the input a at $\pm b$. Running the segmentation without the clipping function caused instability in some of the masses for the T_{DC} component. The overall segmentation threshold is given by

$$T(\theta) = T_{DC} + T_{AC}(\theta), \quad (4)$$

and the level set speed function (in the polar domain) is

$$F_{r,\theta} = sign\left(P_{r,\theta} - T_{r,\theta} \right) H\left(\phi_{r,\theta} - \gamma \right), \quad (5)$$

where $T_{r,\theta} = T(\theta)$. The second term in eq. (5) keeps the level set from segmenting radially more than $\gamma = 20$ pixels outwards from the current segmentation, but it does not constrain the level set if the boundary is moving radially inwards toward the seed point.

Feature extraction is performed using the original mammographic image after level set segmentation is completed and the segmentation has been converted from the polar to the Cartesian domain. Two feature sets are extracted, set I and II. These features are detailed in Table I. Feature set I contains patient features, morphological features, features extracted from the normalized radial length (NRL), and statistical gray level features. Feature set II contains the features in feature set I, plus the textural features created from the segmentation boundary (spatial grey level dependence (SGLD) SB features) and the rubber band straightening transform (RBST) (SGLD RBST features). The RBST is generated with an outward radius of 40 pixels and inward radius of 40 pixels. In order to create the SGLD features, the mammograms are quantized with N=20 quantization levels. Details of standard features may be found in the citations listed in Table I.

A leave-one-out (LOO) methodology is used to perform classification [29]. In this method, one patient's data is used for testing, while all of the other patients' data form a training set which is used to train the classifier. This process repeats in a round-robin order for each patient. A near-optimal feature set is selected from the training set and are analyzed using stepwise linear discriminant analysis (SLDA), with forward selection and backwards rejection, using the ROC A_Z metric [30-32] to select a combination of features that maximizes this metric [1,11,22,29,33]. The SLDA implementation details may be found in [32] (see footnote 1). Although this method does not use an exhaustive search, the SLDA method provides a good compromise for feature selection. Since a LOO methodology is used, for each case there are 59 training cases. In order to keep from overtraining, we limited the SLDA number of features selected to ten.

A k-nearest neighbor (K-NN) classifier [34] is used to classify the SLDA optimally weighted features from the LOO testing sample, and the system efficacy is measured with ROC analysis, overall accuracy, and the number of true positives (TP), false positives (FP), true negatives (TN), false negatives (FN) [30,31]. The values of k in the k-NN

classifier were varied in order to asses the role this parameter played.

V. Experimental Results and Conclusions

Fig. 3 shows 14 representative cases, along with the segmentation results, as well as the physician supplied ROI. Table II shows the *k*-NN classifier results (OA, TP,TN,FP,FN, as well as overall A_Z values with confidence intervals.) Table III shows comparisons of the proposed results (ALSSM) to several previous studies that used the DDSM database. Overall, the ALSSM results outperformed most of the CAD systems listed in the table. However, for a truly fair comparison, each system should be tested on the same set of mammograms.

Mass segmentation in digital mammography is a difficult task. A semi-automated procedure was performed to determine the original seed point in the mammogram based on the physician ROI. The ALSSM method was implemented. Two sets of features were extracted, and a *k*-NN classifier was used to classify the results as malignant or benign. The best results were from feature set I (Patient Age, morphological, statistical, and NRL features) and *k*=6,7,8. The ALSSM compared well to previous studies using the DDSM database.

References

[1] B. Sahiner, H.-P. Chan, N. Petrick, M.A. Helvie, and M.M. Goodsitt, "Computerized characterization of masses on mammograms: The rubber band straightening transform and texture analysis," *Medical Physics,* vol. 25, no. 4, pp. 516-526, Apr. 1998.

[2] M.D. Heath and K.W. Bowyer, "Mass Detection by Relative Image Intensity," *Proc. of the 5th Intl. Conference on Digital Mammography*, Toronto, Canada, Jun. 2000.

[3] American Cancer Society, "American Cancer Society: Breast Cancer Facts & Figures 2005-2006," pp. 1-28, 2006. Available: http://www.cancer.org/downloads/STT/CAFF2005BrF.pdf.

[4] D.M. Catarious, "A Computer-Aided Detection System for Mammographic Masses." PhD Dissertation in Biomedical Engineering. Durham, NC: Duke University, Aug. 2004.

[5] D.M. Catarious, A.H. Baydush, and C.E. Floyd Jr., "Incorporation of an iterative, linear segmentation routine into a mammographic mass CAD system," *Medical Physics,* vol. 31, no. 6, pp. 1512-1520, Jun. 2004.

[6] L. Kinnard, S.-C.B. Lo, P. Wang, M.T. Freedman, and M.F. Chouikha, "Separation of Malignant and Benign Masses using Maximum-Likelihood Modeling and Neural Networks," *Proc.- SPIE The Intl. Society for Optical Engineering,* no. Part 2, pp. 733-741, May 2002.

[7] National Cancer Institute, "National Cancer Institute Fact Sheet: Improving Methods for Breast Cancer Detection and Diagnosis," 2006. Available: http://www.cancer.gov/cancertopics/screening /breast.

[8] M. Sameti, R.K. Ward, B. Palcic, and J. Morgan-Parkes, "Texture feature extraction for tumor detection in mammographic images," *Proc. of the 1997 IEEE Pacific Rim Conference on Communications, Computers and Signal Processing (PACRIM)*,

Victoria, BC, vol. 2, pp. 831-834, Aug. 1997.

[9] M. Beller, R. Stotzka, T.O. Mueller, and H. Gemmeke, "An Example-based System to Support the Segmentation of Stellate Lesions," in *BVM - image processing in medicine*: Springer, pp. 475-479, 2006.

[10] J.T. Sample, "Computer Assisted Screening of Digital Mammographic Images." PhD Dissertation in Computer Science. Hattiesburg, MS: The University of Southern Mississippi, Aug. 2003.

[11] J.E. Ball, T.W. Butler, and L.M. Bruce, "Towards automated segmentation and classification of masses in mammograms," *Proc. of the 26th Annual Intl. Conference of the Engineering in Medicine and Biology Society*, San Francisco, CA, vol. 1, pp. 1814-1817, 2004.

[12] A.O. Bilska-Wolak, C.E. Floyd, Jr., L.W. Nolte, and J.Y. Lo, "Application of likelihood ratio to classification of mammographic masses; performance comparison to case-based reasoning," *Medical Physics,* vol. 30, no. 5, pp. 949-958, May 2003.

[13] N. Székely, N. Tóth, L. Lasztovicza, and B. Pataki, "Combining Methods For Mass Detection In Mammograms," *Proc. of the 17th Biennial Intl. EURASIP Conference, BIOSIGNAL 2004*, Brno, Czech Republic, pp. 281-283, 23-25 May 2004.

[14] H.D. Cheng and M. Cui, "Mass lesion detection with a fuzzy neural network," *Pattern Recognition,* vol. 37, no. 6, pp. 1189-1200, Jun. 2004.

[15] J.E. Ball and L.M. Bruce, "Level set segmentation of remotely sensed hyperspectral images," *Proc. of the IEEE Intl. Conference Geoscience and Remote Sensing (IGARSS)*, Anchorage, AL, vol. 8, pp. 5638 - 5642, Jul. 2005.

[16] J.E. Ball and L.M. Bruce, "Level Set Hyperspectral Image Segmentation and Classification via Spectral Band Selection and Optimized Pixel Discrimination Metrics," *IEEE Trans. on Geoscience and Remote Sensing,* 2006 [under review].

[17] J.E. Ball and L.M. Bruce, "Accuracy analysis of hyperspectral imagery classification using level sets," *Proc. of the 2006 American Society of Photogrammetry and Remote Sensing Annual Conference*, Reno, NV, Apr. 2006.

[18] J.E. Ball and L.M. Bruce, "Level Set Hyperspectral Segmentation: Near-Optimal Speed Functions using Band Selection and Scaled Spectral Angle Mapper," *Proc. of the 2006 IEEE Intl. Geoscience and Remote Sensing Symposium*, pp. 2596 - 2600, Jul. 2006.

[19] G.M. te Brake, N. Karssemeijer, and J.H.C.L. Hendriks, "An automatic method to discriminate malignant masses from normal tissue in digital mammograms," *Physics in Medicine and Biology,* vol. 45, no. 10, pp. 2843-2857, Oct. 2000.

[20] E.D. Pisano, E.B. Cole, B.M. Hemminger, M.J. Yaffe, S.R. Aylward, A.D.A. Maidment, R.E. Johnston, M.B. Williams, L.T. Niklason, E.F. Conant, L.L. Fajardo, D.B. Kopans, M.E. Brown, and S.M. Pizer, "Image Processing Algorithms for Digital Mammography: A Pictorial Essay," *RadioGraphics,* vol. 20, no. 5, pp. 1479-1491, 2000.

[21] N. Eltonsy, H.E. Rickard, G. Tourrasi, and A. Elmaghraby, "Morphological concentric layer analysis for automated detection of suspicious masses in screening mammograms," *Proc. of the 26th Annual Intl. Conference of the IEEE Engineering in Medicine and Biology Society (EMBS)* San Francisco, CA, vol. 1, pp. 1279-1282, Sept. 1-5 2004.

[22] H.D. Cheng, X.J. Shi, R. Min, L.M. Hu, X.P. Cai, and H.N. Du, "Approaches for automated detection and classification of masses in mammograms," *Pattern Recognition,* vol. 39, no. 4, pp. 646-668, Apr. 2006.

[23] J.E. Ball, "Three stage level set segmentation of mass core, periphery, and spiculations for automated image analysis of digital mammograms." Ph.D. in Electrical Engineering. Starkville, MS: Mississippi State Univ., May 2007.

[24] J.A. Sethian, *Level Set Methods and Fast Marching Methods: Evolving Interfaces in Computational Geometry, Fluid Mechanics, Computer Vision, and Materials Science*, 2nd ed. Cambridge, UK: Cambridge University Press, 2002.

[25] M. Heath, K.W. Bowyer, D. Kopans, W. Kegelmeyer, R. Moore, K. Chang, and S. Munishkumaran, "Current status of the Digital Database for Screening Mammography," in *Digital Mammography*,

N. Karssemeijer, M. Thijssen, J. Hendriks, and L. van Erning, Eds. Boston, MA: Kluwer Academic Publishers, pp. 457-460, 1998.

[26] U. Bottigli and B. Golosio, "Feature extraction from mammographic images using fast marching methods," *Nuclear Instruments and Methods in Physics Research Section A: Accelerators, Spectrometers, Detectors and Associated Equipment,* vol. 487, no. 1-2, pp. 209-215, Jul. 2002.

[27] M.A. Kupinski and M.L. Giger, "Automated seeded lesion segmentation on digital mammograms," *IEEE Trans. on Medical Imaging,* vol. 17, no. 4, pp. 510-517, Aug. 1998.

[28] R.L. Egan, *Breast Imaging: Diagnosis and Morphology of Breast Diseases.* Philadelphia, PA: W. B. Saunders Co., 1988.

[29] B. Sahiner, N. Petrick, C. Heang-Ping, L.M. Hadjiiski, C. Paramagul, M.A. Helvie, and M.N. Gurcan, "Computer-aided characterization of mammographic masses: accuracy of mass segmentation and its effects on characterization," *IEEE Trans. on Medical Imaging,* vol. 20, no. 12, pp. 1275-1284, Dec. 2001.

[30] M. Kallergi, "Medical Image Analysis Methods," in *The Electrical Engineering and Applied Signal Processing Series*, L. Costaridou, Ed. New York: Taylor & Francis, pp. 433-472, 2005.

[31] J.A. Hanley and B.J. McNeil, "The Meaning and Use of the Area under a Receiver Operating Characteristic (ROC) Curve," *Radiology,* vol. 143, pp. 29-36, Apr. 1982.

[32] A. Agatheeswaran, "Analysis of the effects of JPEG2000 compression on texture features extracted from digital mammograms ". Masters Thesis in Electrical and Computer Engineering. Starkville, MS: Mississippi State University, pp. 20-37, 42-43, Dec. 2004.

[33] N. Petrick, C. Heang-Ping, B. Sahiner, and M.A. Helvie, "Combined Adaptive enhancement and region-growing segmentation of breast masses on digitized mammograms," *Medical Physics,* vol. 26, no. 8, pp. 1642-1654, Aug. 1999.

[34] R.O. Duda, P.E. Hart, and D.G. Stork, *Pattern Classification*, 2nd ed. New York: John Wiley & Sons, 2001.

[35] R.M. Haralick, I. Dinstein, and K. Shanmugam, "Textural features for image classification," *IEEE Trans. on Systems, Man, and Cybernetics,* vol. SMC-3, pp. 610-621, Nov. 1973.

TABLE II
OVERALL RESULTS. THE BEST RESULTS SHOWN IN BOLD (BEST = HIGHEST OVERALL ACCURACY WITH LOWEST NUMBER OF FN). THE FEATURE SETS (I AND II) ARE DEFINED IN TABLE I.

k [1]	FS [2]	OA %	TP	TN	FP	FN	Overall A_Z, CI [2]
1		82	25	24	6	5	
2		82	25	24	6	5	
3		80	25	23	7	5	
4		85	27	24	6	3	
5	I	85	27	24	6	3	0.9687 ± 0.0014
6		**87**	**28**	**24**	**6**	**2**	
7		**87**	**28**	**24**	**6**	**2**	
8		**87**	**28**	**24**	**6**	**2**	
9		85	27	24	6	3	
10		85	27	24	6	3	
1		85	25	26	4	5	
2		85	25	26	4	5	
3		82	24	25	5	6	
4		82	24	25	5	6	
5	II	82	24	25	5	6	0.9708 ± 0.0017
6		83	25	25	5	5	
7		85	26	25	5	4	
8		**87**	**27**	**25**	**5**	**3**	
9		**87**	**27**	**25**	**5**	**3**	
10		**87**	**27**	**25**	**5**	**3**	

[1] k-NN classifier parameter. [2] FS=Feature Set, CI=Confidence Interval

TABLE I
FEATURE LIST

Feature Set		Feature Type and source [1]	(Number of Features) Features [4,5]
I	II		
•	•	Patient age [25]	(1) Patient Age
•	•	Morphological (SB) [4,5]	(14) Area, Axis ratio, Box ratio, Circularity, Convex hull area, Eccentricity, Equivalent diameter, Extent, Extent ratio[2], Major axis length, Minor axis length, Perimeter length, Solidity, Width to height ratio
•	•	Statistical (SB) [22]	(3) Gray Level Mean, Gray level Std. Dev., Gray Level Std. Dev. Ratio[3]
•	•	NRL (SB) [22]	(6) Entropy, Length, Mean, Roughness, Std. dev., Zero Crossing Count
	•	GLCM (SB) [22,32,35]	(144) Energy, Variance, Correlation, Inertia, Inverse Difference Moment, Entropy
	•	GLCM(RBST)[1,22,32,35]	(864) Energy, Variance, Correlation, Inertia, Inverse Difference Moment, Entropy

[1] This column denotes the region from which the features were extracted. DDSM=DDSM database (there is no region, as the patient age is part of the database). SB=segmentation boundary. NRL stands for Normalized Radial Length. RBST=Rubber Band Straightening Transform [1]. GLCM stands for gray level co-occurrence matrix. GLCM is also known as spatial gray level dependence (SGLD). [2] The extent ratio is max(length, height) / min(length, height). [3] the Gray level std. dev. ratio is the ratio of the std. dev. of the gray levels inside the segmentation to the std. dev. of gray levels outside the segmentation boundary and within 200 pixels of the segmentation boundary. [4] The GLCM SB features are calculated at distances $d=\{1,2,4,6,8,10\}$ and directions $\theta=\{0°,45°,90°,135°\}$. There will be a total of 6 GLCM features x 6 distances x 4 angles for 144 features. [5] The RBST features are the same features as the GLCM SB features. The RBST uses a parameter k to choose how many pixels before and after are used to create the normal vector to the boundary [1]. The RBST features are calculated for distances $k=\{2,4,6,8,10,12\}$ For each value of k, there will be 144 features generated. Therefore there are $864 = 144$ x 6 features.
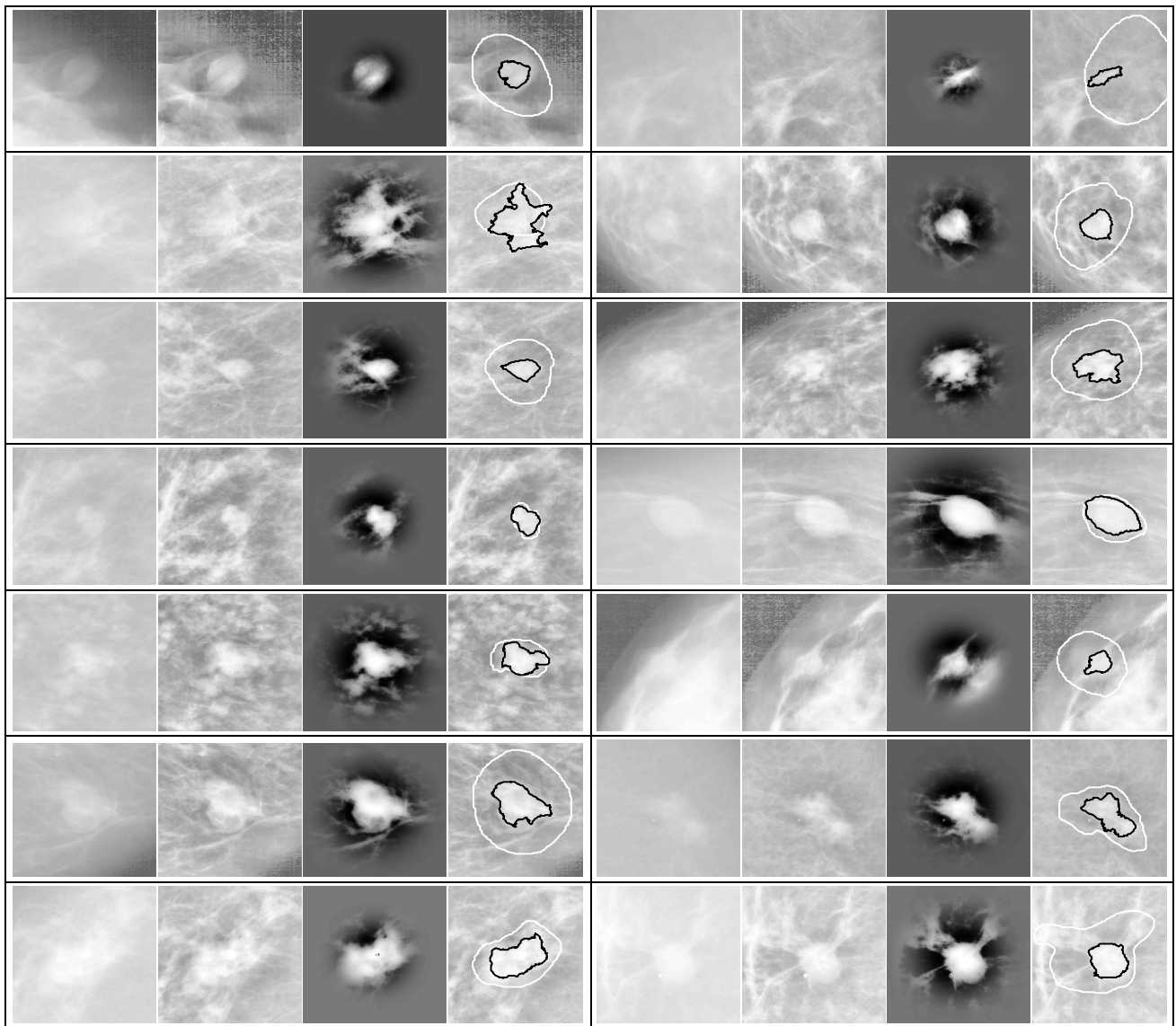
Fig. 3. Images and segmentation results for selected cases. Left-to-right: Original mammogram image, CLAHE enhanced image, level set segmentation enhanced image, CLAHE enhanced image with overlays of the DDSM ROI (white line), ALSSM (the proposed) segmentation (black line).

TABLE III
RESULTS FOR PREVIOUS STUDIES USING THE DDSM DATABASE.

Author and Reference	Results	Author and Reference	Results
ALSSM (Proposed method)	87% OA, 2 FP	Heath and Bowyer [2]	~ 0.7 TPF @ 2 FPPI
Catarious *et al.* [4,5]	93% OA	Kinnard *et al.* [6]	Az = 0.66 to 0.84
Beller *et al.* [9]	70% OA	Sample [10]	~ 80% @ 2.68 FPPI
Bilska-Wolak *et al.* [12]	At 98% sensitivity, spares ~50% of benign biopsies	Szekely *et al.* [13]	0.90 TPF
Cheng and Cui [14]	0.92 TPF @ 1.33 FPPI	te Brake *et al.* [19]	0.90 TPF @ 1.0 FPPI
Eltonsy *et al.* [21]	85.7% TPF		